Hindawi
Geofluids
Volume 2022, Article ID 8382493, 13 pages
https://doi.org/10.1155/2022/8382493

Research Article

Study on the Dynamic Instability Mechanism of the Rock Formation in the Multifault Structure Zone of the Stope

Hanxiao Guo,[1] **Weijian Yu**,[1,2] **Yong Liu**,[3] **Zongtang Zhang**,[4] **and Xiangtao Kang**[3]

[1]*School of Resource, Environment and Safety Engineering, Hunan University of Science and Technology, Xiangtan, Hunan 411201, China*
[2]*Hunan Provincial Key Laboratory of Safe Mining Techniques of Coal Mines, Hunan University of Science and Technology, Xiangtan, Hunan 411201, China*
[3]*College of Mining, Guizhou University, Guiyang, Guizhou 550003, China*
[4]*Hunan Provincial Key Laboratory of Geotechnical Engineering for Stability Control and Health Monitoring, Hunan University of Science and Technology, Xiangtan 411201, China*

Correspondence should be addressed to Weijian Yu; ywjlah@163.com

Received 21 August 2021; Accepted 24 February 2022; Published 29 March 2022

Academic Editor: Dan Ma

Under the influence of tectonism in geological activities, most fault structures appear in groups. Multiple fault structures can induce a variety of mine dynamic disasters, which significantly affect the safety of mine production. To study the dynamic instability mechanism of the strata in the multifault structure zone of the stope when mining, a numerical model of multiple fracture structures was established. At the same time, the mechanism of the dynamic instability of the rock formation in the multifault structure zone of the stope has been studied through similar simulation experiments and on-site data analysis. The research results show that the stress-affected areas of the faults in the multiple-fault structure area overlap, and the stress evolution law of the fault will distinguish its independent dynamic evolution model. The multifault structure area has a multifault overall evolution law model. In this model, there is a synergy between the fault layers, and the maximum value of stress concentration is diagonally distributed. Under the influence of mining, the fault structure will be activated to change the stress field distribution form of the stope. The two faults in multiple structural areas have a joint mechanism, which plays a key role in controlling the dynamic instability process of the surrounding rock of the stope. The first activated faults in the multiple-fault structure area will undergo secondary activation under the influence of subsequent fault activities. The evolution law of cracks in the overburden of similar simulation experiments confirms that the early active F1 fault will be affected by the subsequent F2 fault activity. The mine pressure data measured on-site verifies the reliability of the numerical simulation experiment and the similar simulation experiment.

1. Introduction

The fault is one of the important factors causing the mine dynamic disaster. Theoretical research on the mechanism of the impact of faults on coal mines is the research hotspot of mine dynamic disasters [1–4]. There are many mountainous structures in southwest China, which are affected by tectonic action in geological activities, and fault structures are developed and mostly appear in groups [5]. Therefore, it is of great significance to study the mechanism of mine dynamic disasters induced by multiple fault structures for mine production safety. Due to technical and economic constraints, most of the small faults are gradually excavated in the process of roadway excavation and mining. At the same time, the solutions are often proposed for the current fault problems, and the interaction mechanism of adjacent faults is rarely considered due to the timeliness of mining. The previous active fault will change the surrounding rock stress state and the active influence range of the adjacent fault. The activation of the second fault will amplify the influence and range of activity of the first fault. The rock mass affected by multiple fracture structures is broken and has low

mechanical strength. At present, under the influence of in situ stress and mining disturbance, problems such as the deformation of surrounding rock of the mining roadway and the instability of the overlying rock layer have become more and more prominent. It makes the transportation and operation of mining equipment very difficult to deform and even causes roof fall accidents. Faults are one of the geological structures frequently encountered in mining activities. The existence of faults destroys the continuity and integrity of the rock formations. It is an important factor affecting the safety of coal mining. Many mine disasters such as rock shock, mine water inrush, and stepped subsidence of the ground are caused by the activation of faults caused by mining.

Han et al. [6] established a mechanical model of fault activation when mining on hang-wall and foot-wall mining based on the theory of key strata and deduced the criterion of fault slip and instability. The movement model of key strata is shown in Figure 1. Wang et al. [7] studied the crack areas of overlying strata affected by reverse faults and discovered the characteristics of easy slicing of coal walls in the areas affected by faults. Wu et al. [8] conducted a similar simulation, taking the coal pillar away from the fault as a variable, and concluded that the width of the coal pillar plays a key role in the stability of the surrounding rock of the fault. Li et al. [9] revealed the dynamic change indexes of displacement and stress after fault activation under similar simulation through the data recording of measuring points in the model. Zhang et al. [10] obtained the variation law of stability of faulted rock mass after failure by studying the process of rock mass expansion and dilatancy. Hudson et al. [11] found that the stress near the structural plane is caused by the joint action of the structural plane itself and the surrounding rock mass. Atsushi Sainoki et al. [12–14] studied the influence of joints on the activation of faults by means of simulations and obtained the law of action of different factors on the activities of mining over faults.

Xiao et al. [15] pointed out that the surrounding rock with a developed geological structure and loose and broken will suffer from strong tectonic stress when the coal seam is mined. The surrounding rock of the roadway is characterized by asymmetric deformation and failure, large floor heave deformation, and inner squeezing of two sides. Through field investigation, numerical simulation, and theoretical analysis, Yu et al. [16, 17] studied the action mechanism of fissures on roadway surrounding rock, which has an important guiding role in the study of the failure law of roadway surrounding rock in the fracture zone of fault. Gou et al. [18] simulated the instability process of overlying rock when mining on the fault zone to grasp the movement characteristics of the overlying strata near the fault mining roadway. The test results show that the fault activation is caused by the mining of coal seam, which makes the strata movement have discontinuity, and the roof separation occurs. When the mining roadway is close to the fault, vertical cracks appear on the roadway side, the failure depth of floor increases, the deformation of the roof is not coordinated, and the deformation of the boundary coal pillar is large. Wang et al. [19] found that large mining height, poor mechanical properties of coal and rock mass, and large roof load were important reasons for coal wall slicing near faults. At the same time, the internal mechanism of coal wall lamination in the working face is revealed, and the discriminant basis of coal wall lamination is established. Wang et al. [20] analyzed the top plate stress distribution law by establishing an elastic beam model including normal and inverse faults. Based on the Mohr-Coulomb criterion, the failure mechanism and mechanical mechanism of the roof under different roof loads, different support strengths, and different span-to-height ratios are revealed. Li et al. [21] analyzed the distribution characteristics of the in situ stress field in China's coal mining areas and the relationship between the in situ stress field and fault activity by using 219 groups of measured in situ stress data optimized by regression analysis. The conclusion indicates that 0.6 is the appropriate criterion for fault slip instability in the overall evaluation of fault stability in coal mining areas of China. Wei et al. [22] analyzed the layout of roadway preexcavation and the rationality of the technology when the working face passed through the fault by applying the theory of key strata. The characteristics of mine pressure in the preexcavation roadway at fault position are pointed out, and the optimal supporting parameters are selected by numerical simulation. Wang et al. [23, 24] obtained the failure law of surrounding rock under different confining pressures in the process of coal mining through experimental research, providing theoretical guidance for the failure form of surrounding rock under different confining pressures when mining across faults. Through experiments and theoretical analysis, Ma et al. [25–28] studied the fracture propagation form of overlying rock in stope and the water conduction law of the fracture, which provided an important theoretical basis for the study of fault fracture failure mechanism. Lai et al. [29] observed the microstructure and distribution of cracks (pores) of coal and rock samples adjacent to the fault and measured the physical and mechanical properties of the coal and rock mass. The effect of faults on dynamic pressure in stope was explored through the physical experiment and the numerical simulation. The analysis shows that the existence of fault blocks the continuity of the medium and causes energy to accumulate at the fault. When the work is advancing towards the fault area, the accumulated energy is released and transferred, resulting in the roof of the mining roadway being cut off, coal wall slicing, partial support fracture, and other phenomena.

Experts and scholars have carried out a lot of research work on rockburst under the influence of faults by means of physical experiments, theoretical derivation, and numerical simulation. A series of important indexes representing the relationship between fault and rockburst are revealed, which provides a useful reference for mine safety production [30–33]. As one of the important factors to induce the mining response of coal seam, fault poses a great threat to the safe mining of coal mines. Therefore, it is very important to know the development degree and distribution of faults. For a long time, relevant experts at home and abroad have attached great importance to the adverse effects of faults on the safe mining of coal mines, carried out a lot of research

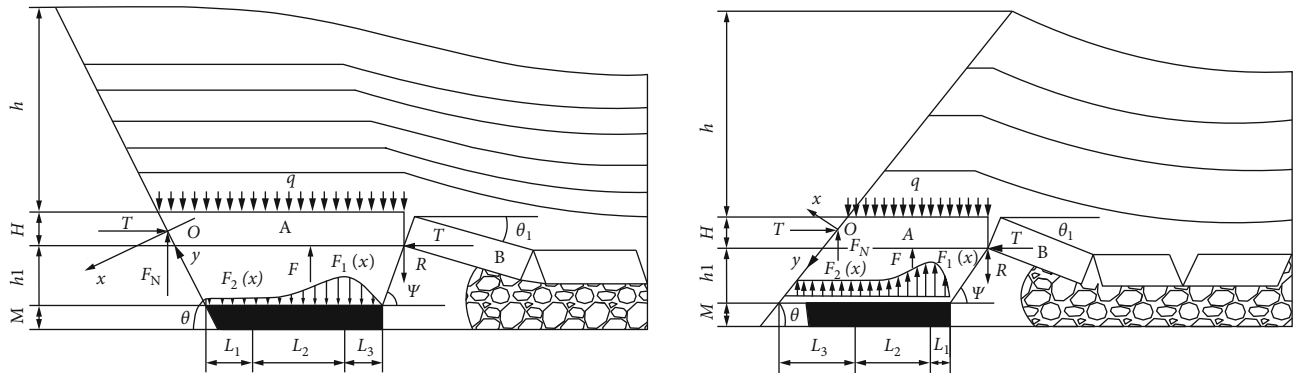

Figure 1: Movement of key strata when mining on hanging-wall and foot-wall [6].

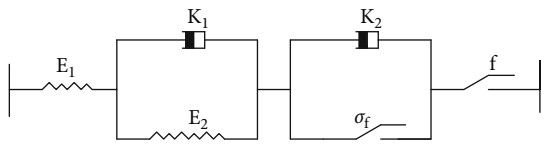

Figure 2: Comprehensive model diagram of rheological instability.

work on this, and achieved fruitful research results [34–37]. At present, most studies focus on a single fault, but few on the joint mechanism of multiple faults. Based on the actual conditions of the specific coal mine, this paper uses a combination of theoretical analysis, numerical simulation, similar simulation, and on-site measurement to study the overburden cracks and stress evolution laws caused by coal mining. The dynamic instability mechanism of rock strata was systematically revealed in the multifault structural area of the stope and provided a reference for the actual production activities.

2. Fault Activation Instability Model

It is rare for the faults to exist alone in nature, and faults often appear in groups during structural changes. Many faults of varying sizes are either almost parallel to each other or intersect or tend to intersect at a certain angle, forming a fault zone. Faults are generated and developed in the process of crustal tectonic changes. Faults are widely distributed in the world and in my country. It is not only an important geological phenomenon related to a series of theoretical issues in structural geology, seismology, and geodynamics. Moreover, it is closely related to the formation and distribution of mineral resources, the foundation stability of large-scale projects, the division of seismic danger zones, and earthquake prediction.

The southwestern region is one of the most widely distributed areas of faults in China. In order to study the dynamic instability mechanism of the strata in the multifault structure zone of the stope, the specific working face of the mining area in Liupanshui, Guizhou, was selected as the research object. By analyzing the mechanical effect of fault, it was found that the rheological instability comprehensive model can explain the activation phenomenon of fault rock well. The model consists of three parts, which can properly describe the viscoelastoplastic mechanical properties of rock. The first part is composed of spring E_1 in series with the Kelvin body, which is mainly manifested as viscoelastic deformation. The viscous element and the friction element are connected in parallel to form the second part and when $\sigma > \sigma_f$ exhibits viscoplastic deformation characteristics. The third part is composed of the friction element, which is used to simulate the phenomenon of sudden sliding when $\sigma > f$. Different rheological instable mechanical phenomena will appear when the σ_f and f values of the model are different. This is shown in Figure 2.

When $\sigma < \sigma_f < f$, the model satisfies the following stress-strain relationship:

$$\begin{cases} \sigma = E_1 \cdot \varepsilon_1, \\ \sigma = E_2 \cdot \varepsilon_2 + K_1 \cdot \varepsilon_2, \\ \varepsilon = \varepsilon_1 + \varepsilon_2. \end{cases} \tag{1}$$

The rheological equation can be obtained from equation (1) as follows:

$$\frac{K_1}{E_1} \cdot \sigma + \frac{E_1 + E_2}{E_1} \cdot \sigma = K_1 \dot{\varepsilon} + E_2 \cdot \varepsilon, \tag{2}$$

where σ and ε represent the differential of stress and strain with respect to time, respectively. When the stress is constant, the following can be obtained:

$$\sigma = \sigma_0 = \cos s \cdot t. \tag{3}$$

And set the initial conditions as $\varepsilon(0) = \varepsilon_0 = \sigma_0/E_1\ (t = 0^+)$. Then, the solution of rheological equation (2) can be changed to

$$\varepsilon(t) = \frac{\sigma_0}{E} + \frac{\varepsilon_0 - \sigma_0}{E} \cdot e^{-t/t_{\text{ret}}}, \tag{4}$$

where $t_{\text{ret}} = K_1/E_2$ is the lag time, $E = E_1 \cdot E_2/E_1 + E_2$.

In summary, when stress is constant, the strain increases with time. Assuming that the strain does not change, that is,

$$\varepsilon = \varepsilon_0 = \cos s \cdot t. \tag{5}$$

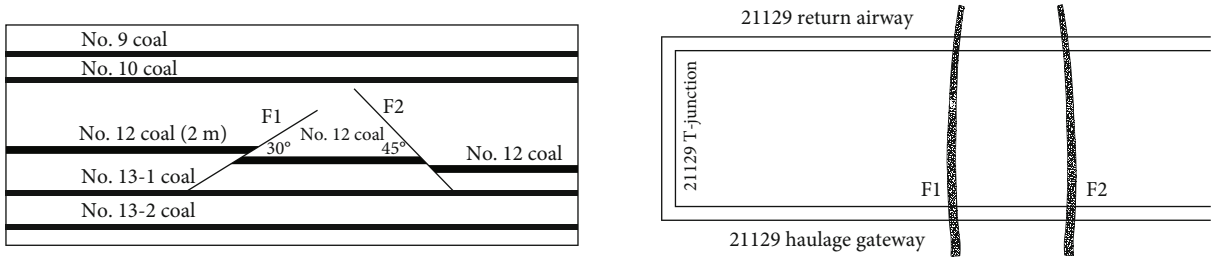

Figure 3: Sketch of the engineering drawing (flat and section).

Table 1: Rock mechanical parameters of each rock layer.

Rock name	Thickness (m)	Bulk (GPa)	Shear (GPa)	$\sigma_{tension}$ (MPa)	Coh. (MPa)	Fric. (°)	Density (kN/m^3)
Siltstone	47	9.94	6.5	2.3	3.2	35	2460
No. 9 coal	1.5	3.22	1.0	0.23	0.6	22	1620
Fine sandstone	2	9.82	6.7	2.5	1.6	32	2660
Siltstone	2	9.94	6.5	2.4	3.2	30	2460
No. 10 coal	0.8	3.22	1.0	0.23	0.6	22	1620
Mudstone	1.5	3.68	3.1	1.8	0.56	20	0.23
Siltstone	4.5	9.94	6.5	2.4	3.2	30	2460
Fine sandstone	22	10.6	9.1	2.0	2.2	32	2200
No. 12 coal	2	4.36	1.2	0.2	0.6	22	1620
Silty mudstone	8	8.16	5.8	1.7	0.7	26	1980
No. 13-1 coal	2	3.22	1.0	0.23	0.6	25	1620
Silty mudstone	5	8.16	5.8	1.7	0.7	26	1980
Fine sandstone	4	10.6	9.1	2.0	2.2	32	2200
No. 13-2 coal	2	3.22	1.0	0.23	0.6	22	1620
Sandy mudstone	5	8.16	5.8	1.7	0.7	26	1980
Siltstone	49	9.94	6.5	2.4	3.2	35	2460

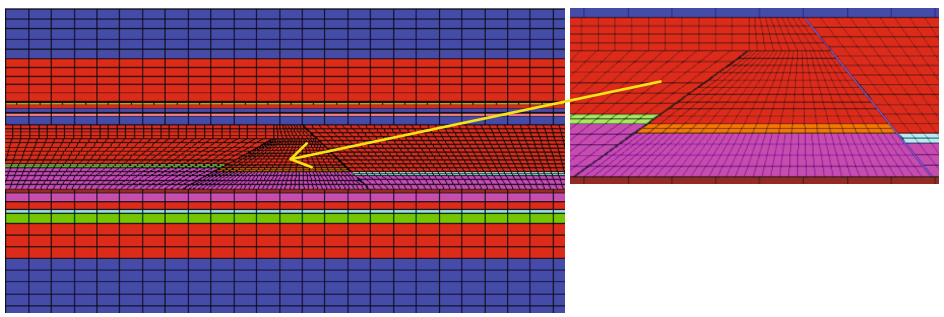

Figure 4: Model and local magnification of the fault.

Then the change of stress with time can be obtained by formula (2) as

$$\sigma(t) = \frac{E_1 \cdot E_2}{E_1 + E_2} \cdot \varepsilon_0 + \frac{{E_1}^2 \cdot \varepsilon_0}{E_1 + E_2} \cdot e^{-t/t_{ret}}, \quad (6)$$

where $t_{ret} = K_1/(E_1 + E_2)$ is the relaxation time, which decreases with the increase of time.

The mining of the working face will have a certain impact on the fault. When the support pressure in the above expression is sufficient, the fault will "activate" and slip. Due to the difficulty in selecting the rock mechanics parameters in the above formulas, the actual engineering calculation is huge. In this paper, numerical simulation and similar simulation are used to study the stress variation in the fault region.

3. Numerical Simulation Analysis of Multiple Fault Zones in Stope

3.1. Model Building. The numerical model established in this paper is based on the geological conditions of the 21 mining area of a coal mine in Guizhou. The average thickness of the No. 12 coal seam excavated by simulation is 2 m, the

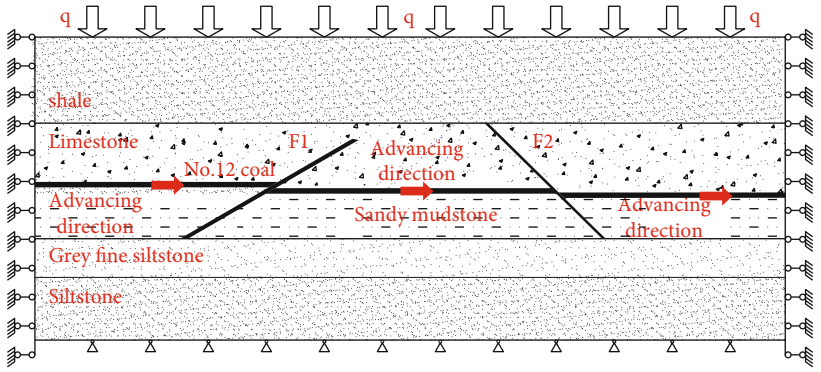

Figure 5: Schematic design of numerical model.

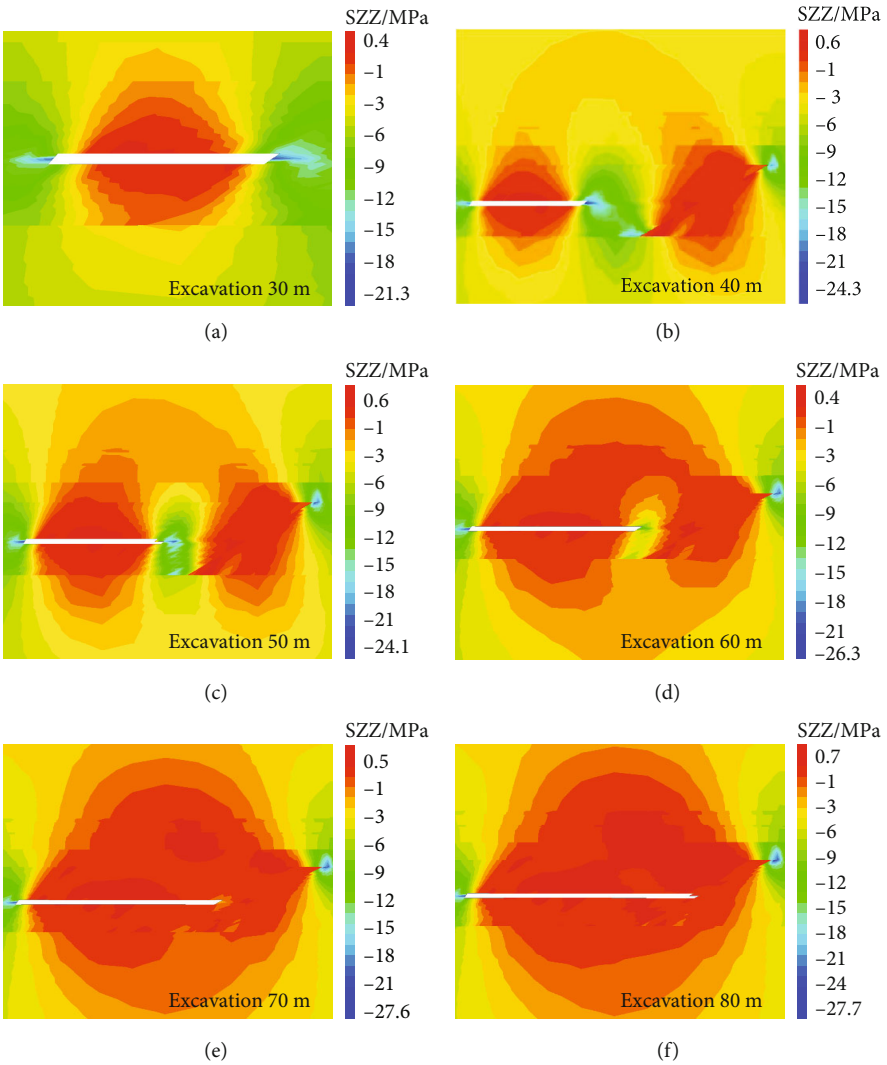

Figure 6: Stress distribution diagram.

inclination is 0°, and the average buried depth is 453 m. In the process of mining, the central part of the working face revealed multiple fault zones composed of F1 and F2 faults. F1 is a reverse fault (dip angle of 30°, drop 2 m), and F2 is a normal fault (dip angle of 45°, drop 2 m). The horizontal distance between the two faults is 62 m in the No. 12 coal seam. According to the measured data of the mine, the strike length, dip length, and height of the model are 340 m, 240 m, and 160 m. According to the measured data of the mine, the strike length, dip length, and height of the model

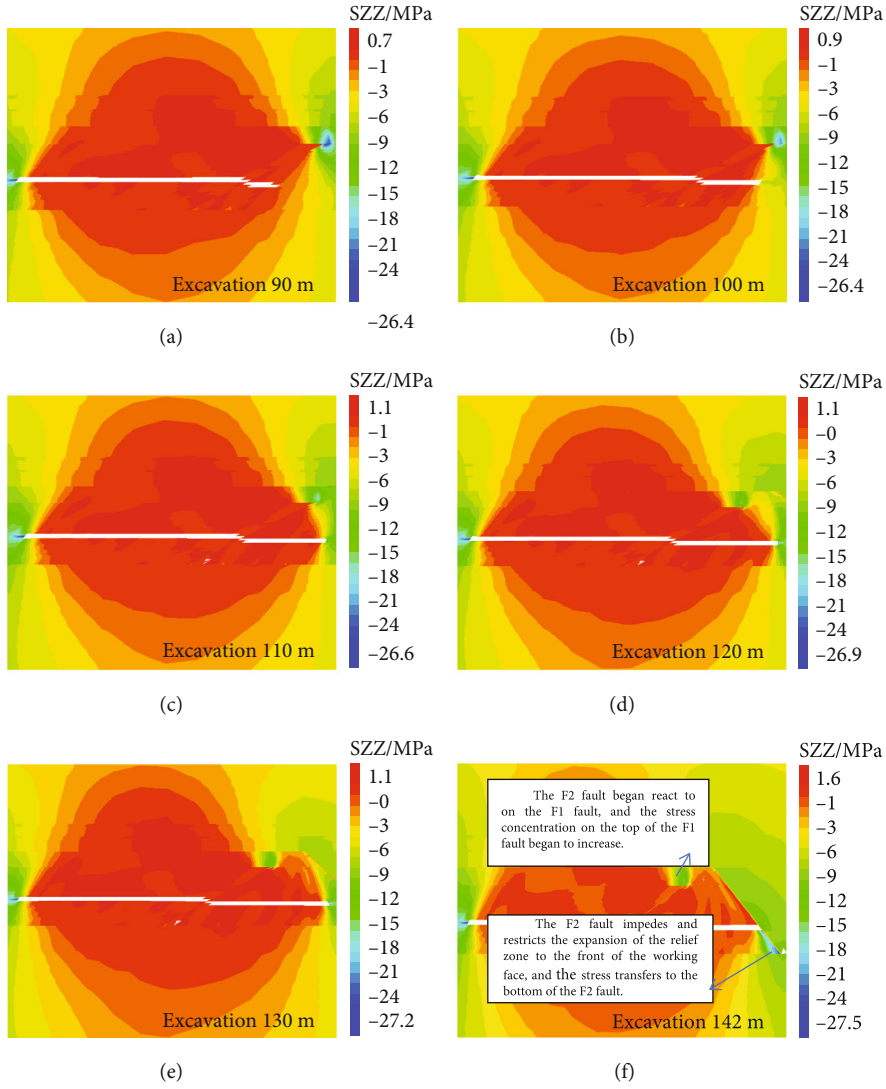

Figure 7: Stress distribution diagram.

are 340 m, 240 m, and 160 m. There is a fracture zone between the upper and footwall of the inverse and normal faults, and the average width of the fracture zone is 0.5 m. Each rock layer is set independently in different layers according to the actual situation. The engineering diagram of the model is shown in Figure 3.

In this model, the Moors-Coulomb model was adopted for rock mass, and the brick element was selected as the basis for modeling [38]. Boundary conditions and initial conditions or model boundary conditions are as follows: fix command is used to fix the velocity components of the boundary nodes in x, y, and z directions. The commands fix x range $x - 0.1$ 0.1 and fix x range x 339.9 340.1 fix the left and right boundaries of the model. The commands fix y range $y -$ 0.1 0.1 and fix y range y 239.9 240.1 fix the front and back boundaries of the model. The command fix z range $z - 0.1$ 0.1 fixes the bottom boundary of the model, and the top of the model is regarded as the free boundary.

The initial conditions of the model stress are as follows: the model height is 160 m, in which the thickness of the overburden of the No. 12 coal seam in the model is 81 m. The actual buried depth of No. 12 coal seam is 453 m, and the overburden pressure of 372 m needs to be compensated by simulation. Taking the bulk density of the rock layer as 28 kN/m^3, the pressure value of overlying rock at 372 m is 10.416 MPa. The horizontal stress coefficient is $\lambda = 1.66$, so the boundary pressure applied around the model is 17.29 MPa. The gravity acceleration $g = 9.8$ m/s^2 should be considered in the whole model. The mechanical parameters of coal and rock mass in the study area are shown in Table 1.

3.2. Simulation Scheme. According to the measured data in the mining area, FLAC^{3D} was used to establish a three-dimensional model, as shown in Figure 4. The measured data and boundary conditions were input to simulate the excavation process. In the simulated 12# coal seam mining, the front and rear protective coal pillars are 40 m, and the left and right protective coal pillars are 50 m. The excavation distance is 10 m for each time. Continue to push forward

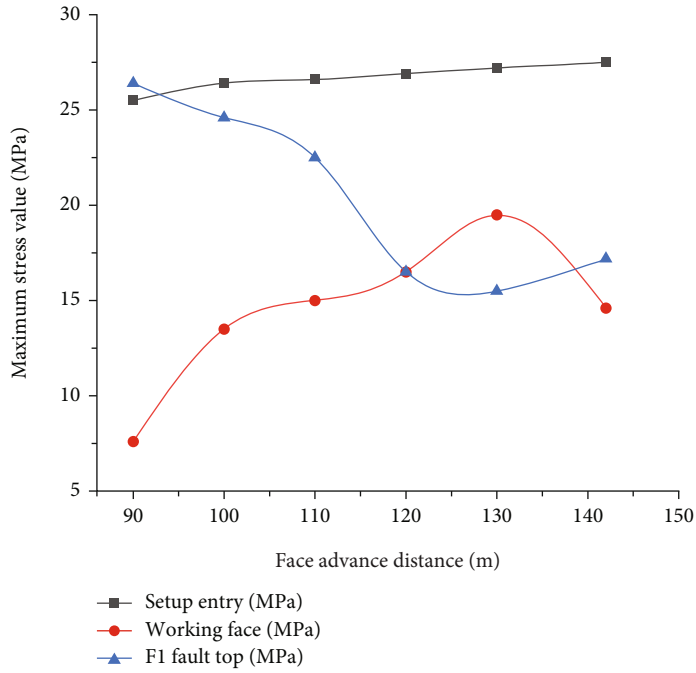

Figure 8: Vertical stress diagram.

after the operation is stable. The mining diagram is shown in Figure 5.

4. Numerical Simulation and Dynamic Analysis of Stope Stress

According to the vertical stress diagram obtained from the simulation, the change of mining stress is systematically described and analyzed.

Stage 1 is from setup entry to F1 (a reverse fault).

As shown in Figure 6(a), the simulated excavation is 30 m, and it is 50 m away from F1, and mining has no effect on the fault basically. The stress concentration appeared in the setup entry and the front of the working face, and their maximum stress values were 21.3 MPa and 20.6 MPa, respectively. The central part of the excavation area is under pressure relief, and the pressure relief height of the upper strata is 22 m.

As shown in Figure 6(b), the working face advances 40 m, and at this time, it is 40 m away from the F1, and the F1 fault begins to have an impact on the working face. The suspension distance of the overlying strata in the goaf reaches the limit span of the old roof fault. The present stress concentration area is formed in the setup entry and the front end of the working face. The stress value of the working face and the setup entry increased obviously, and the maximum stress value was 24.3 MPa and 23 MPa, respectively. The stress reduction zone is formed in the overlying strata of the excavation area, and the pressure relief effect is better at 26.5 m above the roof. At the same time, the stress change occurred in the reverse fault zone, and local pressure relief occurred in the middle part. The stress concentration zones appeared at the upper and lower ends, and the maximum values of the stress concentration zones at the upper and lower ends were 22.5 MPa and 17.5 MPa, respectively. The stress reduction zone appears in the upper-pressure relief zone of the goaf and above the pressure relief zone in the middle of the fault, and the two pressure relief zones are connected in series to form an "n"-shaped pressure relief zone.

As shown in Figure 6(c), the working face advances 50 m, and at this time, it is 30 m away from the F1, and the stress at fault appears to change. At this time, the maximum stress value of the setup entry and the stress concentration area at the front of the working face are 24.1 MPa and 23.7 MPa, respectively. With the increase of excavation range, the value of stress concentration area increases gradually, and the pressure relief area of overlying rock in goaf increases gradually.

As shown in Figure 6(d), the working face advances 60 m. It is 20 m away from F1, and the effect of reverse fault on the roof of the coal seam increases. The stress at the working face and the setup entry is significantly increased. At this time, the maximum stress value of the setup entry and the stress concentration area at the front of the working face are 26.3 MPa and 25.5 MPa, respectively. The roof pressure relief zone in the middle of the excavation area was further extended to 27.3 m above the roof. At the same time, the stress changes in the reverse fault zone, and the maximum values of the stress concentration zones at the upper and lower ends are 23.7 MPa and 17.4 MPa, respectively. The "n"-shaped connected relief zone of the two relief zones at the upper part increases. The "U"-shaped connected relief zones of the two relief zones at the lower part increase, and the two relief zones are connected at the lower part.

As shown in Figure 6(e), the working face advances 70 m, and it is 10 m away from F1. The reverse fault has a significant effect on the surrounding rock of the working

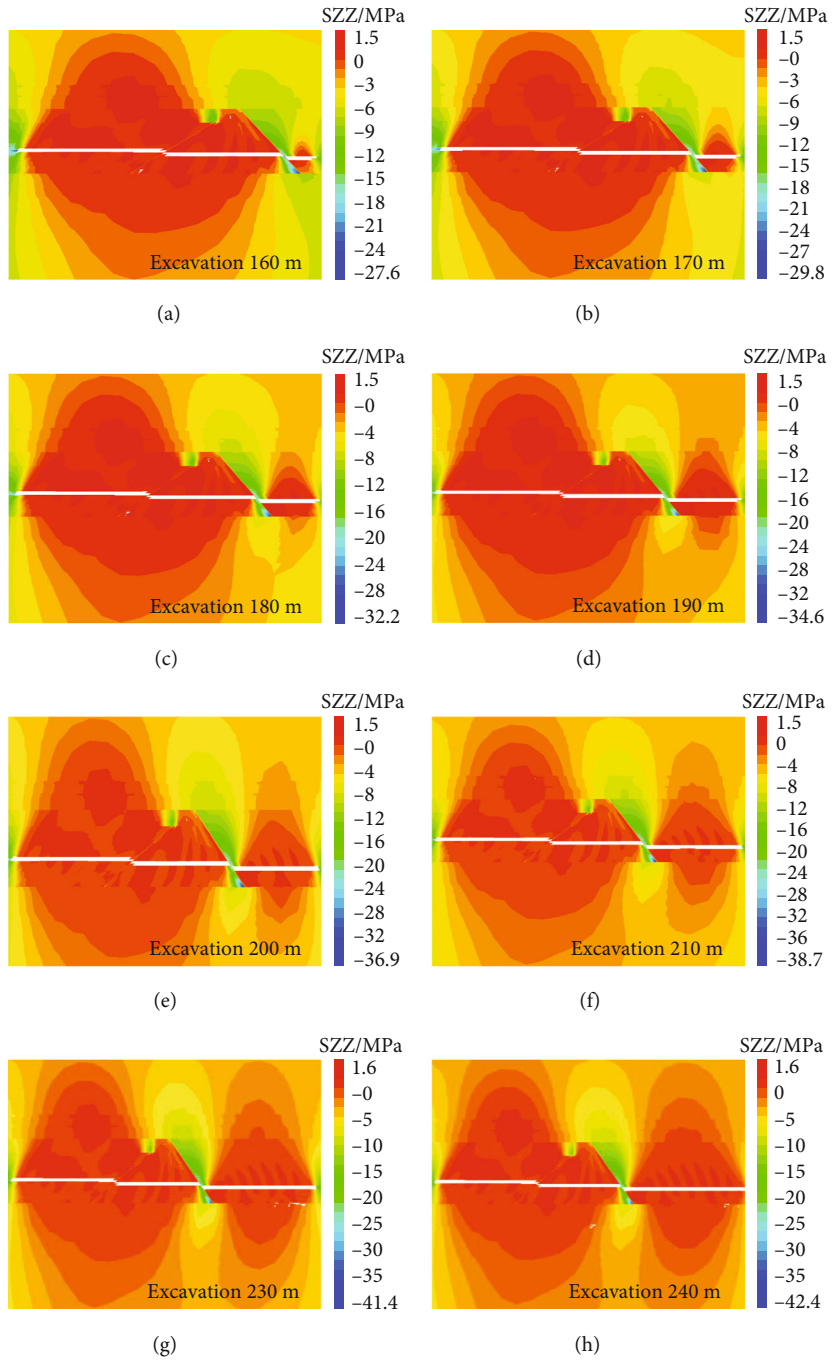

Figure 9: Stress distribution diagram.

face. The maximum stress concentration area at the setup entry is 27.7 MPa, and the stress concentration area at the front of the working face is reduced sharply. At this time, the pressure relief range of the upper strata of the goaf extends to 28.1 m above the roof. At the same time, the stress changes in the reverse fault zone, and local pressure relief occurs in the middle part. The maximum value of the stress concentration zone at the upper end increases to 24.6 MPa, and the lower end is in the pressure relief zone.

As shown in Figure 6(f), the working face advances 80 m, and it is 0 m away from F1 at this time. At this time, the maximum stress value of the setup entry and the stress concentration area at the front of the working face are 27.6 MPa and 5.6 MPa, respectively. At the same time, the maximum value of the stress concentration zone at the upper end of the reverse fault zone is 26.5 MPa, the lower end is in the relief zone, and the relief zone begins to increase in the middle of the fault. The pressure relief area above the goaf

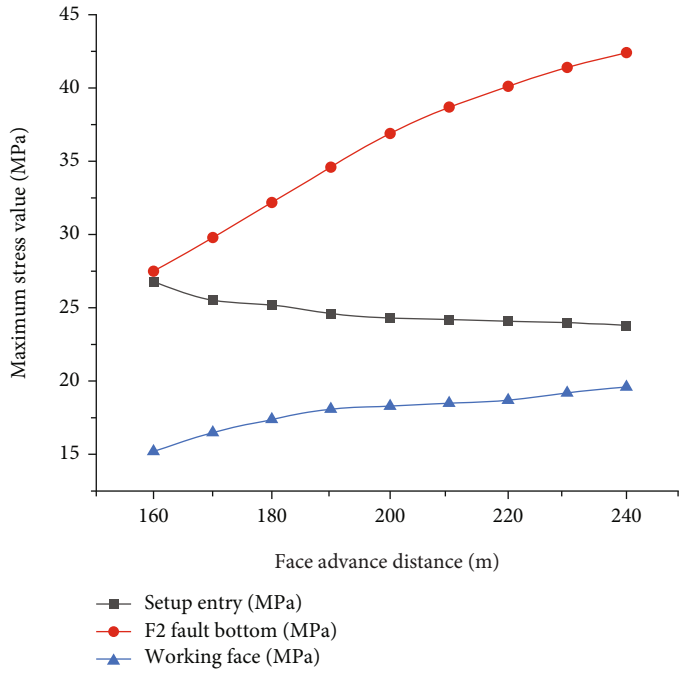

Figure 10: Vertical stress diagram.

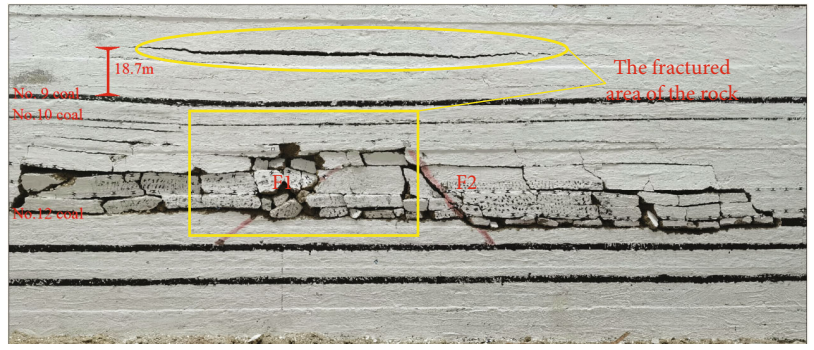

Figure 11: Fracture distribution diagram of similar simulation.

overlapped with the upper plate pressure relief area of F1, and the "n"-shaped pressure relief area above the stope disappeared. The lower pressure relief area of the goaf coincides with the bottom pressure relief area of F1, and the "U"-shaped pressure relief area under the stope disappears.

The second stage is from F1 (a reverse fault) to F2 (a normal fault).

As shown in Figure 7(a), the working face advances 90 m. It is 10 m past the F1 and 52 m away from the F2. F1 reverse fault has a significant influence on the working face, and its effect on the roof of coal seam increases, while normal fault has almost no influence on the working face. The maximum stress concentration area at the setup entry is 25.5 MPa, and there is no obvious stress concentration at the front end of the working face. The pressure relief zone of the goaf surrounding rock is further increased. At the same time, the stress concentration area at the end of the reverse fault zone increases, and the maximum value of stress is 26.4 MPa. The middle part and lower part are in the relief zone.

As shown in Figure 7(b), the working face advances 100 m. It is 20 m over F1 and 42 m away from F2. The F1 reverse fault has a significant influence on the working face, while the F2 normal fault has little influence on the working face. The maximum stress values of setup entry and stress concentration area in front of the working face are 26.4 MPa and 13.5 MPa, respectively. Meanwhile, the maximum value of the stress concentration area at the upper end of the reverse fault is 24.6 MPa.

From the above analysis, it can be seen that in the process of advancing from 80 m to 100 m, the F1 fault and the working face interact greatly, and the F2 fault area is basically stable.

As can be seen from Figures 7(c)–7(f), the advancing distance of the working face ranges from 110 m to 142 m. In this process, the working face is far away from the F1

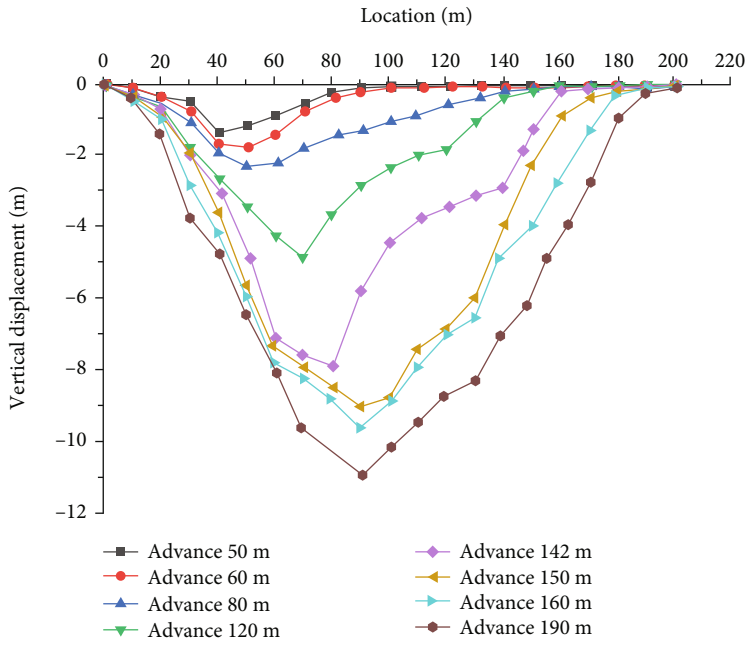

Figure 12: Overburden vertical displacement curve.

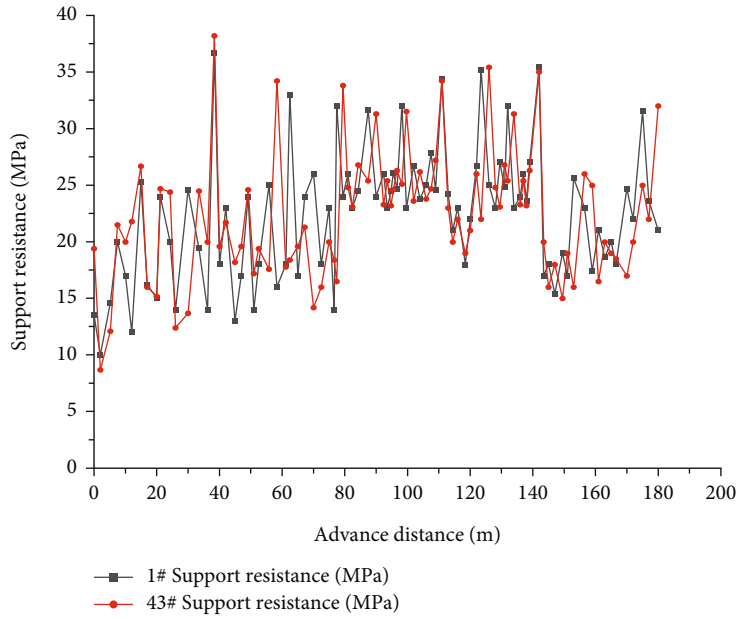

Figure 13: Working resistance curve of hydraulic support.

fault, and the distance from the F1 reverse fault is 30 m-62 m. The working face is close to the F2 fault and the distance from the F2 normal fault is 32 m-0 m. In this process, the influence of fault F1 on the working face gradually decreases, and the interaction between fault F2 and the working face begins to increase [39, 40].

It can be seen from Figure 8 that, within the range of 90 m-100 m, under the influence of the F1 fault, the stress values of the working face and the setup entry changed greatly. With the continuous advancement of the working face, the stress value at the setup entry increases with the increase of the mined-out area. When the advancing distance of the working face is 90 m-130 m, as the distance between the working face and F1 continues to increase, the interaction between F1 and the working face gradually becomes smaller, and the leading support pressure of the working face gradually increases. The F1 fault tends to be stable gradually, and the value of the stress concentration area at the top of the F1 fault decreases gradually. When the working face advances from 130 m to 142 m, the advance bearing stress of the working face suddenly increases from 19.5 MPa to 14.6 MPa, and the maximum stress at the top

of the F1 fault increases from 15.5 MPa to 17.2 MPa. As can be seen from the data changes in Figure 8, the blocking effect of the F2 fault makes the surrounding rock at the front end of the working face at 142 m in the stress reduction zone. At the same time, the activity of the surrounding rock of the F2 fault has an influence on the F1 fault, which intensifies the activity of the F1 fault.

According to Figures 9(a) and 10, the working face advances 160 m. At this time, the working face is 80 m away from the F1 fault and 18 m away from the F2 fault. The stress concentration area is distributed in the setup entry, the lower part of F2, and the front end of the working face. The lower part of the F2 fault shares some of the overburden pressure, which reduces the value of the stress concentration area near the setup entry and the working face. The maximum stress at the cut hole reaches 26.2 MPa, and the maximum stress at the lower part of F2 reaches 27.6 MPa. The maximum stress at the working face is 15.2 MPa. As can be seen from Figures 9(a)–9(h), with the advance of the working face, the F1 fault tends to be basically stable. The value of the stress concentration area from the setup entry is decreasing gradually. The overburden pressure gradually transfers to the lower part of the F2 fault. The maximum stress concentration at the working face increases gradually. Multiple fault structures seriously destroy the continuity of surrounding rock and change the stress distribution of the stope. The multifault structure hinders the stress transfer of the overburdened strata to the working face, which makes the value of the leading abutment pressure of the working face low. Through numerical simulation research and analysis, the role of multiple fault structures in the energy transfer process of the surrounding rock of the stope is obtained. The multicracked structure severely damaged the continuity of the surrounding rock and changed the energy distribution of the surrounding rock. The transfer and concentration of the energy field to the F1 and F2 faults effectively reduce the energy value of the working face.

5. Stope Similarity Simulation Experiment and Field Measurement

As shown in Figure 11, fractures develop in the overlying strata of the goaf in the multifault structural area composed of F1 reverse fault and F2 normal fault, and the rock mass is broken. In particular, due to the multiple effects of mining and F2 fault, the surrounding rock activity in this area is intense, the overlying strata fractures are more developed, and the caving rock mass is more broken. The vertical displacement subsidence of overlying strata in the stope is larger than that of nondouble fault areas on both sides. The vertical displacement curve of overburden is shown in Figure 12. The analysis of the resistance monitoring data of the hydraulic support in the working face shows that the multiple fracture structures can be divided into "high-pressure zone" and "low-pressure zone." The surrounding rock stress in the "high-pressure area" and "low-pressure area" of the fault is abnormal, and the working resistance value of the support in the low-pressure area is higher than that in the nonfault affected area. The working resistance curve of the hydraulic support is shown in Figure 13.

6. Conclusion

By means of finite element numerical simulation software and similar simulation experiment, the movement law of overlying strata and the ore pressure behavior law are studied when 12# coal seam mining passes through multiple fault structure areas. The conclusions are as follows:

(1) The ore pressure behavior law of the surrounding rock of the stope crossing the multiple fault zone was analyzed by the finite element numerical simulation software. The study concluded the following: When the working face passes through the faulting area, the fault has a significant effect on the stress distribution of the surrounding rock. When the working face is 20 m past the F1 fault and advanced to the middle area of multiple fault structures, the pressure relief zone of the surrounding rock in the goaf becomes smaller. The increase of stress concentration area within 10 m in front of the working face is not conducive to the release of gas pressure in front of the working face

(2) During the advancing process of the working face from 80 m (F1 fault) to 142 m (F2 fault), the concentration area and numerical value of the stress at the top of the F1 fault experienced a process of increasing, maximal, decreasing, slowly decreasing, and increasing. The results show that the stress change of the F2 fault promotes the stress change of the F1 fault undermining

(3) When the working face advances to the F2 fault, there is no strong stress concentration in front of the working face due to the blocking effect of the fault. The stress concentration is transferred to the bottom of the F2 fault, which easily causes the floor heave of the working face

(4) Through the numerical analysis of finite element software, it is concluded that the multiple fracture structures will seriously cut the continuity of the surrounding rock and affect the stress distribution of the surrounding rock. Multiple fault structures will only change the energy distribution of the surrounding rock but will not increase the value of energy. The transfer and concentration of the energy field to the F1 fault and the F2 fault effectively reduced the energy value of the working face. This phenomenon provides a new possibility for the study of underground engineering

Data Availability

The experimental test data used to support the findings of this study are available from the corresponding author upon request.

Conflicts of Interest

The authors declare that there are no conflicts of interest regarding the publication of this article.

Acknowledgments

This study was supported by the National Natural Science Foundation of China (Grant Nos. 52174076, 51974117, 51964008, and 52064009), Hunan Provincial Natural Science Foundation of China (Grant No. 2020JJ4027), and Hunan Provincial Graduate Scientific Research Innovation Project (Grant No. CX20210984).

References

[1] Q. MG and S. PW, *Mine Pressure and Rock Formation Control*, China University of Mining and Technology Press, 2003.

[2] P. YS, L. ZH, and Z. MT, "Mechanism and prevention of rockbrust in China," *Chinese Journal of Rock Mechanics and Engineering*, vol. 22, no. 11, pp. 1844–1851, 2003.

[3] Y. D. P. Y. Jiang and J. FuX, "State of the art review on mechanism and prevention of coal bumps in China," *Journal of China Coal Society*, vol. 39, no. 2, pp. 205–213, 2014.

[4] F. Cui, S. Dong, X. Lai, J. Chen, C. Jia, and T. Zhang, "Study on the fracture law of inclined hard roof and surrounding rock control of mining roadway in longwall mining face," *Energies*, vol. 13, no. 20, p. 5344, 2020.

[5] H. FM, *Introduction to Fault Mechanics*, Seismological Press, 2013.

[6] H. KM, Y. QG, Z. HX, and L. FM, "Mechanism of fault activation when mining on hanging-wall and foot-wall," *Journal of China Coal Society*, vol. 45, no. 4, pp. 1327–1335, 2020.

[7] W. A. N. G. Chen, T. U. Shihao, T. U. Hongsheng, B. A. I. Qingsheng, and C. H. E. N. Guanshen, "Rock deformation and support bearing characteristics in reversed fault zone with strata pinchout," *Journal of Mining and Safety Engineering*, vol. 32, no. 2, pp. 182–186, 2015.

[8] J. W. Wu, H. S. Tong, S. J. Tong, and D. Q. Tang, "Study on similar material for simulation of mining effect of rock mass at fault zone," *Chinese Journal of Rock Mechanics and Engineering*, vol. 26, pp. 4170–4175, 2007.

[9] Z. H. Li, C. Z. Zhai, and L. F. Li, "Experimental study on water inrush mechanism due to floor faults activation in mining above confined aquifer," *Journal of Central South University*, vol. 46, no. 5, pp. 1806–1810, 2015.

[10] W. Q. Zhang, Q. Sun, S. Y. Zhu, and D. Q. Liu, "Analysis of roof reverse fault instability-reactivation mechanism under mining," *Coal Safety*, vol. 44, no. 3, pp. 179–182, 2013.

[11] A. HJ and P. HJ, *Engineering Rock Mechanics-An Introduction to the Principles*, Elsevier, 2000.

[12] H. G. Ji, H. S. Ma, J. A. Wang, Y. H. Zhang, and H. Cao, "Mining disturbance effect and mining arrangements analysis of near-fault mining in high tectonic stress region," *Safety Science*, vol. 50, no. 4, pp. 649–654, 2012.

[13] A. Sainoki and H. S. Mitri, "Dynamic behaviour of mining-induced fault slip," *International Journal of Rock Mechanics and Mining Sciences*, vol. 66, pp. 19–29, 2014.

[14] A. Sainoki and H. S. Mitri, "Effect of slip-weakening distance on selected seismic source parameters of mining-induced fault-slip," *International Journal of Rock Mechanics and Mining Sciences*, vol. 73, pp. 115–122, 2015.

[15] T. Q. Xiao, J. B. Bai, J. P. Li, X. Y. Wang, and S. Yan, "Stabilization mechanism of crushed surrounding rock in coal roadway with bolt support near fault," *Journal of Mining & Safety Engineering*, vol. 27, no. 4, pp. 482–486, 2010.

[16] W. Yu, K. Li, Q. Lu, and H. Guo, "Engineering characteristics and deformation control of roadways in fractured rock mass," *Journal of China Coal Society*, vol. 46, no. 11, pp. 1–12, 2021.

[17] W. Yu, G. Wu, and B. An, "Large deformation characteristics and stability control of roadway with fractured rock mass," *Journal of Mining and Safety Engineering*, vol. 36, no. 1, pp. 103–111, 2019.

[18] P. F. Gou and Y. G. Hu, "Effect of faults on movement of roof rock strata in gateway," *Journal of Mining & Safety Engineering*, vol. 23, no. 3, pp. 285–288, 2006.

[19] Z. H. Wang, J. H. Yang, and H. Meng, "Mechanism and controlling technology of rib spalling in mining face with large cutting height passing through fault," *Journal of China Coal Society*, vol. 40, no. 1, pp. 42–49, 2015.

[20] Q. Wang, S. C. Li, Z. Li et al., "Analysis of roof collapse mechanism and supporting measures in fault zone of coal roadway," *Rock and Soil Mechanics*, vol. 33, no. 10, pp. 3093–3102, 2012.

[21] L. P and M. SJ, "Analysis of the characteristics of in-situ stress field and fault activity in the coal mining area of China," *Journal of China Coal Society*, vol. 41, no. S2, pp. 319–329, 2016.

[22] L. W. Wei and D. S. Zhang, "Gateway pre-heading feasibility in fault of coal mining face and support parameter optimization," *Coal Science and Technology*, vol. 32, no. 4, pp. 57–60, 2004.

[23] W. Shao-feng, T. Yu, and W. Shan-yong, "Influence of brittleness and confining stress on rock cuttability based on rock indentation tests," *Journal of Central South University*, vol. 28, pp. 2786–2800, 2021.

[24] W. Shao-feng, T. Yu, L. Xi-bing, and D. Kun, "Analyses and predictions of rock cuttabilities under different confining stresses and rock properties based on rock indentation tests by conical pick," *Transactions of the Nonferrous Metals Society of China*, vol. 31, no. 6, pp. 1766–1783, 2021.

[25] D. Ma, S. Kong, Z. Li, Q. Zhang, Z. Wang, and Z. Zhou, "Effect of wetting-drying cycle on hydraulic and mechanical properties of cemented paste backfill of the recycled solid wastes," *Chemosphere*, vol. 282, p. 131163, 2021.

[26] D. Ma, J. Wanga, X. Cai et al., "Effects of height/diameter ratio on failure and damage properties of granite under coupled bending and splitting deformation," *Engineering Fracture Mechanics*, vol. 220, p. 106640, 2019.

[27] D. Ma, J. Zhang, H. Duan et al., "Reutilization of gangue wastes in underground backfilling mining: overburden aquifer protection," *Chemosphere*, vol. 264, p. 128400, 2021.

[28] H. Wu, D. Ma, A. J. S. Spearing, and G. Zhao, "Fracture reponse and mechanisms of brittle rock with different numbers of openings under uniaxial loading," *Geomechanics and Engineering*, vol. 25, pp. 481–493, 2021.

[29] X. Lai, J. Zheng, J. Chen, X. J. Jiang, B. Chang, and H. H. Zhao, "Comprehensive identification of rock-coal mass internal critical destabilization in fault influenced broken zone," *Journal of China Coal Society*, vol. 40, no. S1, pp. 1–5, 2015.

[30] Z. H. Li, L. M. Dou, Z. Y. Lu, X. W. Lu, and G. R. Wang, "Study of the fault slide destabilization induced by coal mining,"

Journal of Mining and Safety Engineering, vol. 27, no. 4, pp. 499–504, 2010.

[31] Y. X. Xia, J. H. Wang, and D. Mao, "Analysis of fault activation induced rock burst risk based on in-situ stress measurements," *Journal of China Coal Society*, vol. 41, no. 12, pp. 3008–3015, 2016.

[32] Y. Qiuge, Z. Huaxing, and D. Weinan, "Analysis of fault separation generation and its effect on mining zone transferring," *Journal of China Coal Society*, vol. 43, no. 12, pp. 3286–3292, 2018.

[33] L. G. Wang and X. X. Miao, "Numerical simulation of coal floor fault activation influenced by mining," *Journal of China University of Mining and Technology*, vol. 16, no. 4, pp. 385–388, 2006.

[34] B. E. Adler, "Tektonische Deformationszahl zur Gebirgsbeschreibung," *Glückauf*, vol. 114, no. 4, pp. 169–175, 1978.

[35] H. Kose, "Modeltheoretische Untersuchung der Gebirgsdruckverteilung beim Abbau," *Gluckauf-Forschungshefte*, vol. 48, no. 1, pp. 17–22, 1987.

[36] X. YC and H. MX, "GMDH-BP evaluation and prediction method of mine structure and its application," *Journal of China Coal Society*, vol. 22, no. 5, pp. 466–469, 1997.

[37] W. YJ and W. YM, "Influence and control of surrounding rock stress on roadway in fault fracture zone," *Coal Science & Technology*, vol. 2, pp. 35–37, 1999.

[38] P. WB, *FLAC3D Practical Tutorial*, China Machine Press, Beijing, 2007.

[39] J. P. Zuo, Z. H. Chen, H. W. Wang, X. P. Liu, and Z. P. Wu, "Experimental investigation on fault activation pattern under deep mining," *Journal of China Coal Society*, vol. 34, no. 3, pp. 305–309, 2009.

[40] Y. D. Jiang, T. Wang, Y. X. Zhao, and C. Wang, "Numerical simulation of fault activation pattern induced by coal extraction," *Journal of China University of Mining and Technology*, vol. 42, no. 1, pp. 1–5, 2013.